remote sensing

MDPI

Article

Discovering Potential Settlement Areas around Archaeological Tells Using the Integration between Historic Topographic Maps, Optical, and Radar Data in the Northern Nile Delta, Egypt

Abdelaziz Elfadaly [1,2,*], Mohamed A. R. Abouarab [3], Radwa. R. M. El Shabrawy [4], Wael Mostafa [5] Penelope Wilson [6], Christophe Morhange [7], Jay Silverstein [8] and Rosa Lasaponara [1]

1 Italian National Research Council, C.da Santa Loja, Tito Scalo, 85050 Potenza, Italy; rosa.lasaponara@imaa.cnr.it
2 National Authority for Remote Sensing and Space Sciences, Cairo 1564, Egypt; abdelaziz.elfadaly@imaa.cnr.it
3 Department of Archaeology, Faculty of Arts, Kafrelsheikh University, Kafrelsheikh 1501, Egypt; mabouarab@art.kfs.edu.eg
4 Ministry of Antiquities, Cairo 11211, Egypt; Rodee_M2007@hotmail.com
5 Department of Geography, Faculty of Arts, Kafrelsheikh University, Kafrelsheikh 1501, Egypt; waelgeo8@gmail.com
6 Department of Archaeology, Durham University, Durham DH1 4EE, UK; penelope.wilson@durham.ac.uk
7 CEREGE, Collège de France, AMU, Aix-Marseille Université, 13284 Marseille CEDEX 07, France; morhange@cerege.fr
8 School of Advanced Studies, University of Tyumen, 625003 Tyumen, Russia; j.silverstein@utmn.ru
* Correspondence: Italian National Research Council, C.da Santa Loja, Tito Scalo, 85050 Potenza, Italy; abdelaziz.elfadaly@imaa.cnr.it; Tel.: +39-327-709-0396

Received: 25 October 2019; Accepted: 13 December 2019; Published: 16 December 2019

Abstract: The primary objective of this study is to leverage the integration of surface mapping data derived from optical, radar, and historic topographical studies with archaeological sampling to identify ancient settlement areas in the Northern Nile Delta, Egypt. This study employed the following methods: digitization of topographic maps, band indices techniques on optical data, the creation of a 3D model from SRTM data, and Sentinel-1 interferometric wide swath (IW) analysis. This type of study is particularly relevant to the search for evidence of otherwise hidden ancient settlements. Due to its geographical situation and the fertility of the Nile, Egypt witnessed the autochthonous development of predynastic and dynastic civilizations, as well as an extensive history of external influences due to Greek, Roman, Coptic, Islamic, and Colonial-era interventions. Excavation work at Buto (Tell el-Fara'in) in 2017–18, carried out by the Kafrelsheikh University (KFS) in cooperation with the Ministry of Antiquities, demonstrated that remote sensing data offers considerable promise as a tool for developing regional settlement studies and excavation strategies. This study integrates the mission work in Buto with the satellite imagery in and around the area of the excavation. The results of the initial Buto area research serve as a methodological model to expand the study area to the North Delta with the goal of detecting the extent of the ancient kingdoms of Buto and Sakha. The results of this research include the creation of a composite historical database using ancient references and early topographical maps (1722, 1941, 1950, and 1997), Optical Corona (1965), Landsat MSS (Multispectral Scanner System) (1973, 1978, and 1988), TM (Thematic Mapper) (2005) data, and Radar SRTM (2014) and Sentinel1 (2018 and 2019) data. The data in this study have been analyzed using the ArcMap, Envi, and SNAP software. The results from the current investigation highlight the rapid changes in the land use/land cover in the last century in which many ancient sites were lost due to agriculture and urban development. Three potential settlement areas have been identified with the Sentinel1 Radar data, and have been integrated with the early maps. These discoveries will help develop excavation strategies aimed at

elucidating the ancient settlement dynamics and history of the region during the next phase of research.

Keywords: buried sites; ancient civilizations; northern Egyptian kingdom; GIS techniques; big data; Space Archaeology; Remote Sensing Survey

1. Introduction

In Egypt, two different predynastic cultures practiced agriculture during the 4th millennium B.C: the Nagada culture in the south and the Buto-Maadi culture in the north. Evidence of early settlements of the Nagada is preserved, with much of the interpretation of the evolution of socio-political complexity derived from burial contexts. It has been proposed that neolithic agriculture spread from north to south, while early states formed first in the south; however, there is insufficient data to support this hypothesis [1]. Major settlements in Upper Egypt between Qena and Luxor and in Lower Egypt indicate that the predynastic period was defined by the political centralization of Egyptian neolithic cultures dating approximately between 4500 BCE and 3000 BCE [2,3]. Furthermore, the Neolithic period and the Predynastic and Early Dynastic eras were part of a World System network connecting Africa, Mesopotamia, the Levant, and Asia Minor. The united Egyptian state (Northern and Southern kingdoms) in the Early Dynastic period (c. 3100 BCE) begins a sequence of more than 500 kings divided into thirty dynasties ending with the arrival of Ptolemaic kings and Roman emperors [4].

Historically, the Nile was divided into several branches (seven branches were known in the 1st century AD), and the large alluvial plain between Cairo and the Mediterranean Sea assumed its present form during the middle Holocene (ca. 7000 BP) [5–7]. While archaeological evidence from the Nile Delta has clearly demonstrated that the area had been inhabited before the dynastic era [8], there are insufficient data to interpret the influences on the Nile Delta on the development of Egyptian culture [9,10]. This has led to speculation that the delta developed states only due to the influence of Upper Egypt, and for some researchers to even suggest that the Nile Delta could have been largely uninhabited until dynastic times [11]. Recently, a number of discoveries in Lower Egypt proved the existence of inhabited centers in the region that had complex links with Western Asia. In fact, rather than playing a marginal role in the development of Egyptian culture, new evidence is demonstrating the importance of Lower Egypt in the birth of Egyptian civilization [12]. Some of the most important data for the predynastic civilization of north Egypt comes from Tell el-Farkha where a brewery complex was excavated in the early nineties [13]. Yet, despite important discoveries, exceptional challenges related to land-use and urban development make systematic studies of early settlement in Lower Egypt problematic. To address this problem, we have used a multifaceted application of historic records and various areal imaging technologies to assess settlement locations.

In the last decades, satellites have offered new opportunities to monitor climate change, urbanization, looting, and site destruction. Archaeologists have used satellite images since the early 1980s [14,15], as well as both aerial and other space platforms, mainly operated by the National Aeronautics and Space Administration (NASA) researchers [16]. Beginning with aerial photos, optical satellite remote sensing (passive data) has played an important role in the field of archaeological investigation over much of the last century [17–23]. Recently, archaeological investigations conducted using SAR data (active data) have moved remote sensing surveys forward to another stage, focusing on archaeological detection and monitoring using backscattering change [24,25]. Concerning SAR data, the European Space Agency (ESA) launched the C-band Sentinel-1A satellite in April 2014, and Sentinel-1B in April 2016 [26]. Sentinel-1 data can give valuable information to feed into researches of landscape archaeology and large-area monitoring activities [27].

Unfortunately, the rapidly-increasing modern population has led to a sprawl of urban and cultivated areas in Egypt that has negatively affected many ancient sites (ancient buildings and koms,

or tells) [28], especially in the Nile Delta, where approximately 80% of the Egyptian population lives. This threat has prompted many researchers to focus their studies on archaeological sites in the Nile Delta using remote sensing and GIS techniques [29–31]. These studies identified over 700 archaeological sites in the Delta Nile (about 200 potential sites are beneath the modern towns). Many of these buried features are visible only when the acquired satellite images are collected at the right time of year to control variables of cloud cover, moisture, and cropping [32–38].

On the other hand, older and recent topographic maps provide useful data for archaeological studies, such as the study of Karl W.Butzer "Early Hydraulic Civilization in Egypt" [39]. The digitization and analysis of these historic maps can help to define archaeological sites within their natural environment and to determine the characteristics of archaeological settlements supporting the development of hypotheses regarding the settlement pattern and environment that are testable through excavation [40–42]. Data from the ancient maps, georeferenced with verified GPS points of the archaeological sites, are essential in the production of accurate scientific archaeological maps [43]. Generally, this study is focused on highlighting the advantage of using the integration between the historic topographical maps, Optical Landsat data, and the Radar Sentinel-1 data in archaeological and heritage studies. In more detail, the ancient topographic maps, Corona, Landsat satellite MSS, TM images, and SRTM data can give an accurate vision of the landscape in Egypt in the last Century and the Sentinel-1 radar data.

The integration, analysis and interpretation of all of these datasets is addressed to improve our knowledge about Tells in the Northern Nile Delta in Egypt with the primary goal of detecting the extents of the ancient kingdoms of Buto and Sakha, and, therefore, to expand the study area to the North Delta. This is undertaken by performing a landscape classification to identify geomorphological units with more potential to contain archaeological evidence (from settlements to burials and all sorts of evidence) and identify potential buried buildings which can reveal ancient settlement areas in the captured satellite images. Finally, correlating ancient topographic maps and remote sensing data (e.g. optical and radar data) can help to expand our understanding of the settlement history of the delta when correlated with archaeological data that verifies image interpretation and provides chronological control. This preliminary study is a further step, building on the work of the EES (Egyptian Exploration Society) Delta Survey, the EAMENA (Endangered Archaeology in the Middle East and North Africa) project, and the work of other researchers in developing a methodology to address the lack of data related to the evolution of socio-political complexity in the Nile Delta.

Study Area

By 7000 years ago, the Nile Delta fluvium had formed into the basic geomorphological form it currently has, although it was riven with numerous dynamic channels which were regularly remodeled by annual flooding [44,45]. The study area is located in the middle of Kafr El-Sheikh governorate, in the northwestern portion of the Nile Delta, between 30° 51' 00" – 30° 55' 30"E, and 31° 15' 00" – 31° 21' 00"N. Climatically, the study area is characterized by a semi-arid, Mediterranean climate [46]. The study area is covered by large zones of cultivated land, some small towns, and eight archaeological koms or mounds (el Khanziri, Nashaween, el Khawaleed, El Garad, el Ineizi, el Dabaa1, el Dabaa2, el Khirba) (Figure 1).

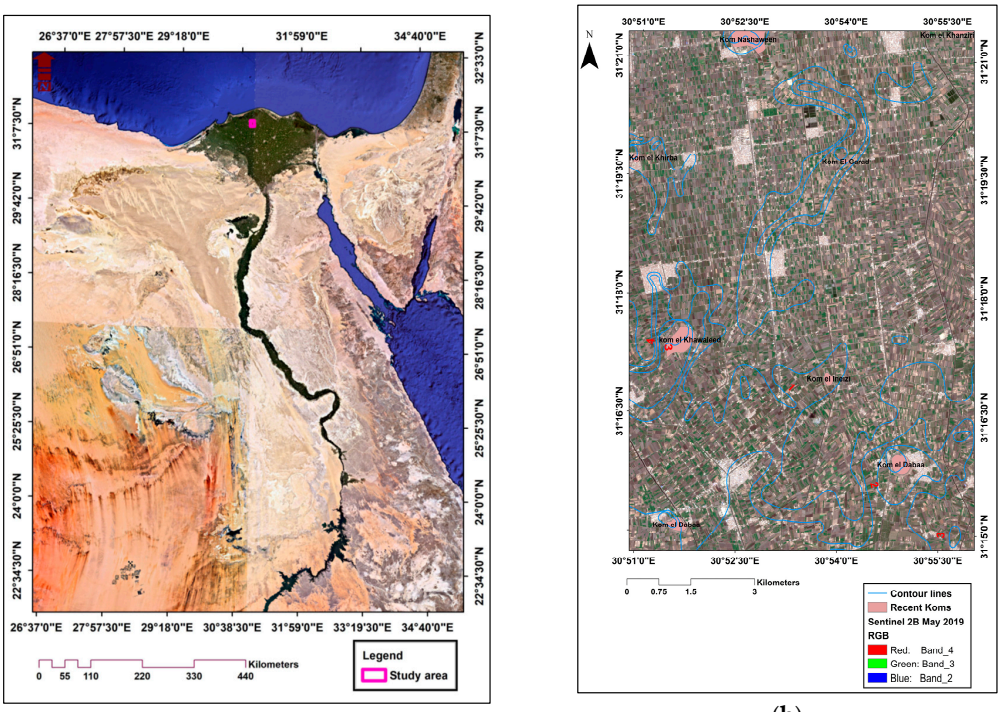

(**a**) (**b**)

Figure 1. Shows the location of the study area: (**a**) Egypt using Google Earth image; (**b**) The study area using Sentinel-2B May 2019 (RGB 4, 3, 2).

2. Materials and Methods

2.1. Materials

This study used the archives of the British Library 1722 topographic map, the American War Office 1941 topographic map with a scale of 1:100000, the topographic maps of the Egyptian General Survey Authority published in 1950 with a scale of 1:25000, and the topographic maps of the Egyptian General Survey Authority published in 1997 with a scale of 1:50000, to identify topographic features and to detect natural and anthropogenic changes in study area. Also, SRTM, Corona Jan 1965, the Landsat satellite images MSS May 1973, MSS May 1978, MSS May 1988, and TM May 2005 were used to define elevation and vegetation values for the various layers in the study area. The current SRTM, Corona, and Landsat archive are accessible from the USGS earth explorer [47]. Radar data from Sentinel-1 from 5 May 2018, and Sentinel-1B captured on 22 May 2019, were selected because May offered clear visibility and it is in the harvest season in Nile Delta (Table 1). The current Sentinel-1A/B archive is accessible from the Sentinel Scientific Data Hub [48]. The topographic maps and SRTM data were rendered using the tools available in the ArcMap 10.4.1 software. Optical satellite imagery processing was done using tools available in Envi 5.1 and ArcMap 10.4.1 software. The Sentinel application platform (SNAP 6.0) software was used for processing the Sentinel-1 data. The analyses were used to detect potential buried settlement areas through georectification of digitized images, analysis of features in the radar data, and band-combination techniques of the past data (Figure 2).

Table 1. The raw data properties of the study include the topographic maps, optical, and radar data.

Raw data	Sensor	Scale/Resolution	Acquisition date	Source

Topographic Maps	–	–	1722	British Library Board
	–	1:100000	1941	American War Office
	–	1:25000	1950	Egyptian General Survey Authority
	–	1:50000	1997	
Optical Data	Corona J-1 (KH-4A)	2.75 m	Jan 1965	USGS (Earth Explorer)
	Landsat MSS	60 m	May 1973	
	Landsat MSS	60 m	May 1978	
	Landsat MSS	60 m	May 1987	
	Landsat TM	30 m	May 2005	
Radar data	SRTM	1-ARC Second Global 30 m	Sep 2014	USGS
	Sentinel 1A	Level-1 GRD (IW) 20x22 m	May 2018	ESA (data scientific hub)
	Sentinel 1B	Level-1 GRD (IW) 20x22 m	May 2019	

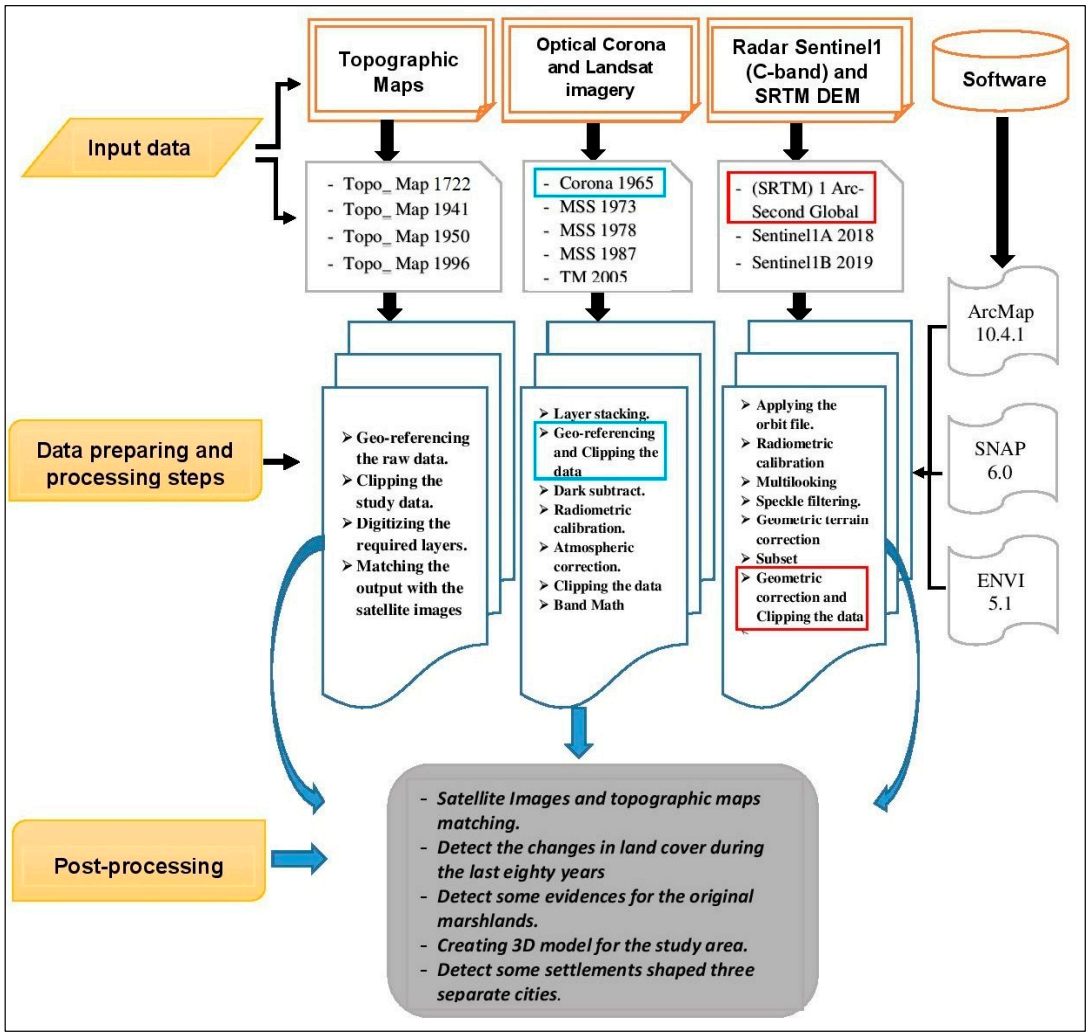

Figure 2. The flowchart includes the input data (Satellite images and maps), the software used, the methods and processing steps, and the results of the study.

2.2. Methods

2.2.1. Digitizing the Topographical Maps

Topographic map sheets were scanned and the raw data were geographically corrected using the georeferencing tool (add control points) in ArcMap software based on the projection coordinate system WGS_1984_UTM_Zone_36N [49]. The registered topographic maps were aligned with the georeferenced satellite images (Landsat) for assessment of the accuracy of the referenced data. The topographic maps were clipped according to the area of interest of the study area to facilitate processing speed. The required thematic layers (e.g. points, lines, and polygons) were defined according to identifiable features on the GIS and created in a geodatabase. All topographic map analyses were completed using the GIS software (ArcMap 10.4.1).

2.2.2 Preparing the Corona Data

The study area was downloaded from the USGS official site according to the optimal dates of coverage from the Corona database. The raw data was then georeferenced and georectified to the projection coordinate system WGS_1984_UTM_Zone_36N. The registered Corona data was matched with the referenced Landsat satellite images for assessment of the accuracy of the referenced data. Finally, the Corona satellite image was clipped according to the study area.

2.2.3. Band Indices

Landsat Multi-Spectral Scanner (MSS) and Thematic Mapper (TM) images were geometrically corrected, calibrated, and removed from their dropouts. Histogram equalization enhancement techniques were also performed on each image to improve the quality of the data. According to the differences in the band-designations of the two sensors (Landsat MSS and TM data) [50], the band properties for the collected data were taken into consideration before applying the band combination method (Table. 2 and Table 3).

Table 2. Band-designations for the used bands for implementation the formula in Landsat Multispectral Scanner (MSS1-5).

Landsat MSS 1–3	Landsat MSS 4–5	Wavelength (micrometers)	Resolution (m)
Band 4 - Blue	Band 1 - Blue	0.5-0.6	60
Band 5 - Green	Band 2 - Green	0.6-0.7	60
Band 6 - Red	Band 3 - Red	0.7-0.8	60
Band 7 - Near Infrared (NIR)	Band 4 - Near Infrared (NIR)	0.8-1.1	60

Table 3. Band-designations for the used bands for implementation the formula in Landsat Thematic Mapper (TM4, 5).

Landsat Thematic Mapper (TM4, 5) Bands	Wavelength (micrometers)	Resolution (m)
Band 1	0.45-0.52	30
Band 2-Green	0.52-0.60	30
Band 3-Red	0.63-0.69	30
Band 4-Near Infrared (NIR)	0.76-0.90	30
Band 5-Shortwave Infrared (SWIR) 1	1.55-1.75	30
Band 7-Shortwave Infrared (SWIR) 2	2.08-2.35	30

In this study, the original marshlands and barren areas of the northern delta were detected according to four kinds of band indices by measuring the vegetation values. The band combinations were extracted from Landsat MSS and TM imagery. The first method used was the Global Environmental Monitoring Index (GEMI), which is produced by Equation (1) [51]. This formula was carried out using the combination of NIR and red bands in the Landsat MSS and TM data.

$$\begin{aligned}((NIR)\text{^}2\ -\ (Red)\text{^}2\ )\ *\ 2\ +\ ((NIR)*\ 1.5)\ +\ ((((Red)*\ 0.5)))/((\ (NIR)+(Red)\\ +\ 0.5)\ )\ *\ (1\ -\ ((NIR)\text{^}2-(Red)\text{^}2\ ))\ *\ 2\ +\ ((\ (NIR)\ *\ 1.5)\\ +\ (Red)\ *\ 0.5))/(((NIR)+\ (Red)+\ 0.5)\ *\ 0.25)))-\ ((\ (Red)\\ -\ 0.125)/(1\ -\ (Red)\ ))\end{aligned} \quad (1)$$

The second method used was the Enhanced Vegetation Index (EVI2), which was determined using the combination of red and green bands in Landsat MSS and TM data by Equation (2) [52].

$$2.5*(((\text{Red})-(\text{Green})))/(\ (\text{Red}) + 2.4\ *(\text{Green}) + 1))) \quad (2)$$

The third method used was the Green Normalized Difference Vegetation Index (GNDVI) [53]. This method parsed the data according to Near-Infrared and Green bands in Landsat MSS and TM satellite images according to the Equation (3).

$$((\text{NIR} - \text{Green}))/((\text{NIR} + \text{Green})) \quad (3)$$

The fourth method used a soil-adjusted vegetation index (OSAVI). This method is developed by [53]. This formula was carried out using a combination of red and green bands in Landsat MSS and TM data (4).

$$(((\text{Red})-(\text{Green})))/((\text{Red})+(\text{Green})+\ 0.16)))*\ (1+0.16) \quad (4)$$

2.2.4. Preparing the Radar SRTM Data

After downloading the Shuttle Radar Topography Mission (SRTM) 1 arc-second data, the raw data were geometrically corrected based on the WGS_1984_UTM_zone_36N projection coordinate system. Then, the SRTM data was clipped according to the area of interest. Using the ArcMap software, the disparity in the topography of the earth in the study area was detected using SRTM data.

2.2.5. Sentinel1 Processing

The study used Sentinel-1A/B (C-band) interferometric wide (IW) swath mode with the mode products at SAR Level-1 Ground Range, Multi-look, detected in May 2018 and 2019. The data product is available in single polarization (HH or VV) for IW mode. Level-1 Ground Range Detected (GRD) products consist of focused SAR data that has been detected, multi-looked, and projected to ground range using an Earth ellipsoid model WGS84 [54]. The ellipsoid projection of the GRD products was corrected using the terrain height specified in the product general annotation. The terrain height used varied in azimuth but was constant in range. The resulting product has approximate square spatial resolution pixels and square pixel spacing with reduced speckle [55]. The data processing steps were analyzed using Apply Orbit File, Radiometric Calibration, Multilooking, Speckle Filtering, and Geometric Terrain Correction as follows:

- Apply Orbit File

Sentinels Precise Orbit Determination (POD) service provides orbit products containing satellite state vectors with an accuracy of a few centimeters. Sentinel-specific processing facilities host the relevant Level-1 instrument processor components and precise orbit determination [56], and provide accurate satellite position and velocity information for correcting geometric distortion. According to the analyses performed on a set of Sentinel-1 data, the orbit products provided (resituated and precise orbits products) meet the expected accuracy. In general, the expected accuracy of "resituated orbits" is enough for computing interferograms without artifacts [57].

- Radiometric calibration

Radiometric correction of an image was carried out so that the pixel values truly represented the backscattering of the reflecting surface. After data preprocessing, the calibrated data were filtered to reduce SAR inherent speckle noise and clipped in range and azimuth in order to remove image border noise. The result of the preprocessing is a reprojected, radiometrically-calibrated, and rescaled normalized radar cross-section (NRCS) image [58]. The radiometric calibration was applied using Equations (5-12) [59]:

$$value(i)=|DN\_i\ |^2/(A\_i^2\ ) \quad (5)$$

where, depending on the selected Look Up Table (LUT),

$$value(i)=\text{one of } ⟦\beta\_i⟧^0, ⟦\sigma\_i⟧^0 \text{ or } \gamma\_i \text{ or originalDN\_i.} \quad (6)$$

$$A\_i=\text{one of betaNought (i),single Nought t(i) ,gamma(i) or dn(i)} \quad (7)$$

Bi-linear interpolation should be used for any pixels that fall between points in the LUT.

Level-1 products provide a noise LUT for each measurement data set. The values in the denoise LUT, provided in linear power, can be used to derive calibrated noise profiles matching the calibrated GRD data. The denoise LUT must be calibrated matching the radiometric calibration LUT applied to the DN:

$$noise(i)=\eta\_i/(A\_i^2) \quad (8)$$

where depending on the LUT selected to calibrate the image data,

$$noise(i)=\text{calibrated noise profile for one of} ⟦\beta\_i⟧^0, ⟦\sigma\_i⟧^0 \text{ or } \gamma\_i \text{ or originalDN\_i.} \quad (9)$$

$$\eta\_i=\text{noiseLut (i).} \quad (10)$$

$$A\_i=\text{one of betaNought (i),single Nought t(i) ,gamma(i) or dn(i)} \quad (11)$$

The calibrated noise profile can be applied to remove the noise by subtraction. Application of the radiometric calibration LUT and the calibrated denoise LUT can be applied in one step, as follows:

$$value(i)=((DN\_i^2-\eta\_i))/(A\_i^2) \quad (12)$$

- Multilooking

After radiometric calibration, the spatial resolution was degraded, but the image noise was reduced, and approximate square pixel spacing was achieved. Therefore, the Multilooking technique tool in the SNAP software was required to reduce the speckle noise effect, reaching a spatial resolution of 20 m [60].

- Speckle filter

Furthermore, speckle filtering was needed to suppress the noise and to remove observations that were not affected by noise and that contained valuable land surface information (e.g. soil moisture and biomass extent). In this study, the single product speckle filter method in SNAP was used to remove the speckle. The SNAP Sentinel-1 Toolbox operator supports the speckle filter types for handling speckle noise of different distributions (Gaussian, multiplicative or Gamma): Mean, Median, Lee, Refined Lee, and Gamma-MA. Therefore, the Refined Lee filter was applied because it maintains the detail of the standing boundary [61].

- Geometric Terrain correction

Finally, the geometric correction ("Range-Doppler Terrain Correction" module in the SNAP) required conversion of the Sentinel-1 GRD data from slant range geometry into a map coordinate system [62]. In more detail, terrain correction was applied to accurately geocode the images by correcting SAR geometric distortions (foreshortening, layover, and shadow) using the digital

elevation model from the Shuttle Radar Topography Mission (that allows us to take into account the local elevation variations) for geocoding SAR imagery [63]. Therefore, the images were overlaid, without additional coregistration. The Range Doppler Terrain Correction (RDTC) operator implemented the Range-Doppler orthorectification method accordingly [64].

3. Results

3.1. Detect Changes in Land Use/Landcover

Change detection analysis described and quantified the differences between the topographic map layers of the same area using manual digitizing (calculate geometry) in the ArcMap software from a diachronic series of reference maps. The different acquisition dates (1941, 1950, and 1997) made it possible to detect the changes in the cultivated area (marshlands) and barren-lands (sabkha and built-up lands) over a period of 56 years. The classified topographic maps of the three dates were used to calculate the area of different land covers and observe the changes that are taking place during the time span of the data. In more detail, the analysis of topographic maps in 1941, 1950, and 1997 revealed that cultivated lands in 1941 covered about 26.8 km² in the target area, and that barren land covered 72.6 km². In 1950, the cultivated land covered about 32.3 km², and barren land about 67.1 km². By 1997, the cultivated area covered about 90.1 km², and barren land 9.3 km² (Figure 3a–d).

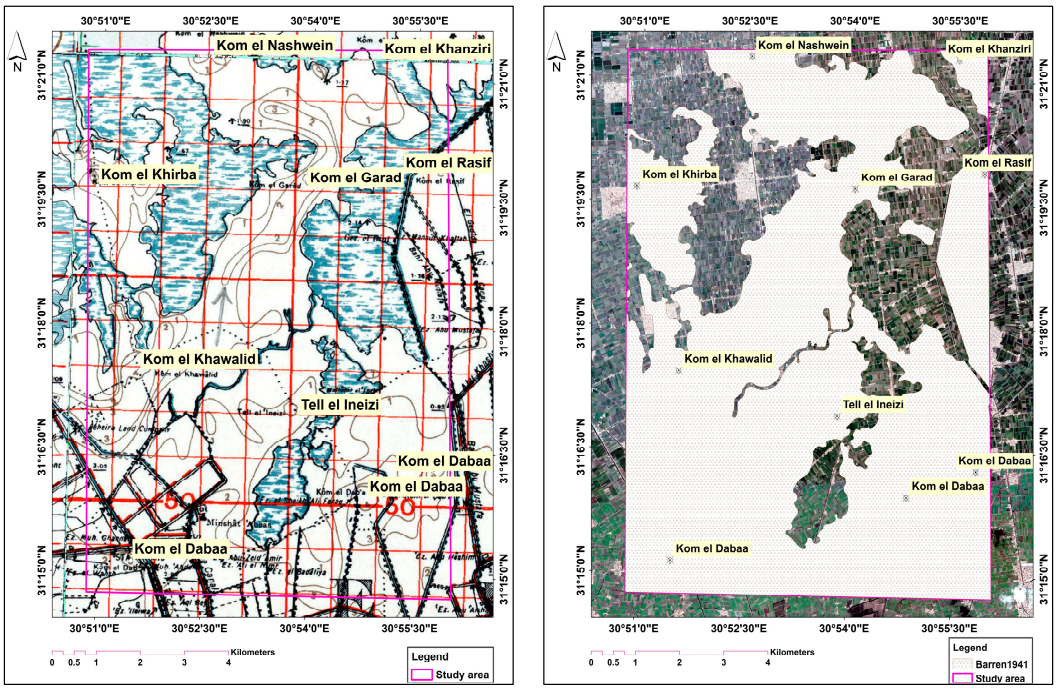

(**a**) (**b**)

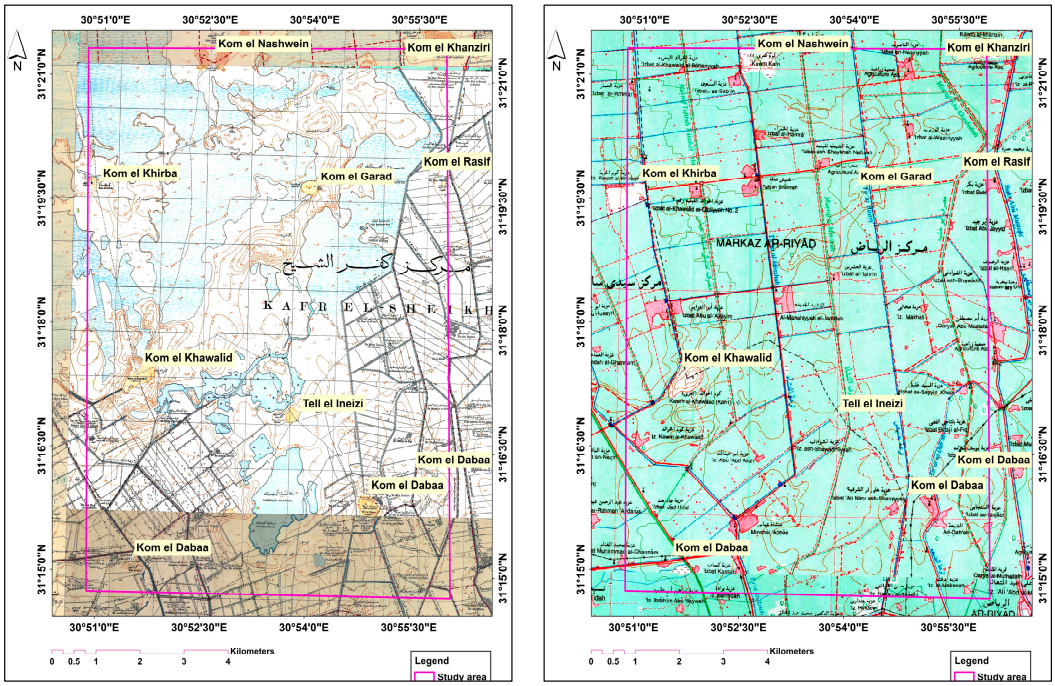

Figure 3. Shows the changes in the land use/land cover in the study area using topographic maps: (**a**) topographic map with scale 1:100000 according to the American war office published in 1941; (**b**) The extent of the barren area according to the topographic map in 1941 using Google Earth image in 2018; (**c**) Topographic map with scale 1:25000 according to the Egyptian General Survey Authority published in 1950; (**d**) Topographic map with scale 1:50000 according to the Egyptian General Survey Authority published in 1997.

3.2. Detection of the Ancient Marshlands by Remote Sensing Indices

In this study, band combination techniques were used to identify barren lands and ancient marshlands, according to the vegetation value (between 0 and 1) in the investigated satellite imagery dating between 1973 and 2005. The assessment included four indices; Enhanced Vegetation Index (EVI2) applied in Landsat satellite image MSS 1973, the Green Normalized Difference Vegetation Index (GNDVI) applied in Landsat satellite image MSS 1978, a soil-adjusted vegetation index (OSAVI) applied in Landsat satellite image MSS 1988, and the Global Environmental Monitoring Index (GEMI) applied in Landsat satellite image TM 2005. These remote sensing indices served as proxy indicators to assess the differences in the vegetation value between the original marshland and barren area in the study area. By using the combinations of the relevant indices (EVI2, GNDVI, OSAVI, and GEMI), we were able to identify the original marshlands and barren areas of the northern delta. The different indices maps are very close each other, but for each year, each index can provide slight enhancements in land use mapping, also depending on the types of changes that occurred. As a whole, the results of the remote sensing indices showed that the marshlands identified correlated significantly with the historic topographic maps; for the sake of brevity, and to be more informative, Figures 4 show the (a) EVI2 index as obtained from Landsat satellite image MSS 1973; (b) the GNDVI index, as obtained from Landsat satellite image MSS 1978; (c) the OSAVI index, as obtained from Landsat satellite image MSS 1988; (d) the GEMI index, as obtained from Landsat satellite image TM 2005.

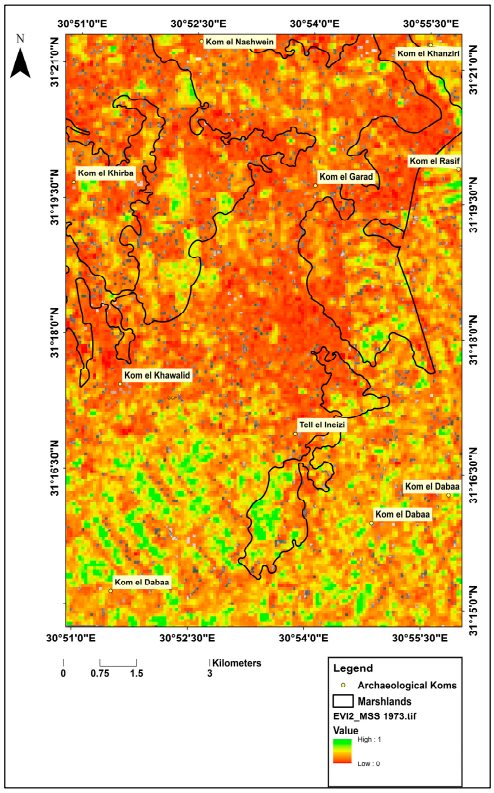
30°51'0"E
30°52'30"E
30°54'0"E
30°55'30"E
N
31°21'0"N
31°19'30"N
31°18'0"N
31°16'30"N
31°15'0"N
Kom el Nashwein
Kom el Khanziri
Kom el Khirba
Kom el Garad
Kom el Rasif
Kom el Khawalid
Tell el Inezi
Kom el Dabaa
Kom el Dabaa
Kom el Dabaa
0 0.75 1.5 3 Kilometers
Legend
Archaeological Koms
Marshlands
EVI2_MSS 1973.tif
Value
High : 1
Low : 0

(**a**)

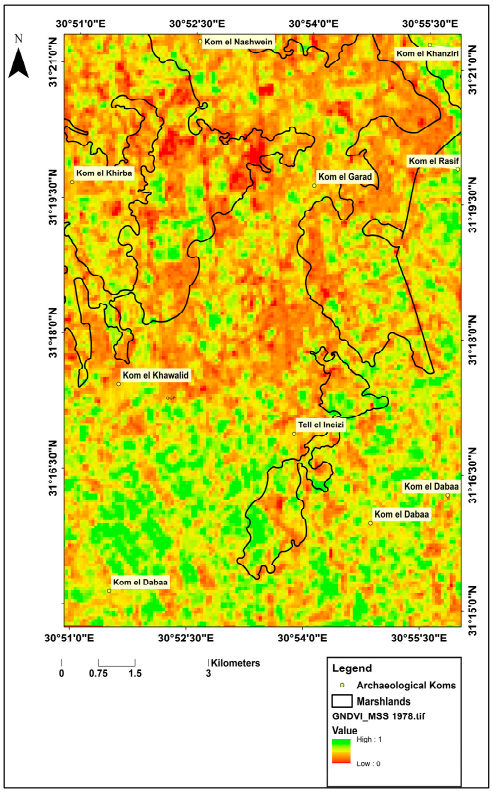
30°51'0"E
30°52'30"E
30°54'0"E
30°55'30"E
N
31°21'0"N
31°19'30"N
31°18'0"N
31°16'30"N
31°15'0"N
Kom el Nashwein
Kom el Khanziri
Kom el Khirba
Kom el Garad
Kom el Rasif
Kom el Khawalid
Tell el Inezi
Kom el Dabaa
Kom el Dabaa
Kom el Dabaa
0 0.75 1.5 3 Kilometers
Legend
Archaeological Koms
Marshlands
GNDVI_MSS 1978.tif
Value
High : 1
Low : 0

(**b**)

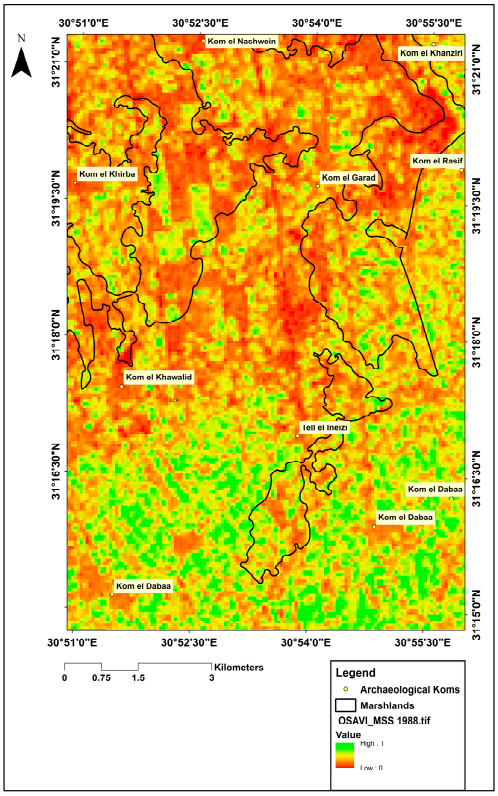
30°51'0"E
30°52'30"E
30°54'0"E
30°55'30"E
N
31°21'0"N
31°19'30"N
31°18'0"N
31°16'30"N
31°15'0"N
Kom el Nashwein
Kom el Khanziri
Kom el Khirba
Kom el Garad
Kom el Rasif
Kom el Khawalid
Tell el Inezi
Kom el Dabaa
Kom el Dabaa
Kom el Dabaa
0 0.75 1.5 3 Kilometers
Legend
Archaeological Koms
Marshlands
OSAVI_MSS 1988.tif
Value
High : 1
Low : 0

(**c**)

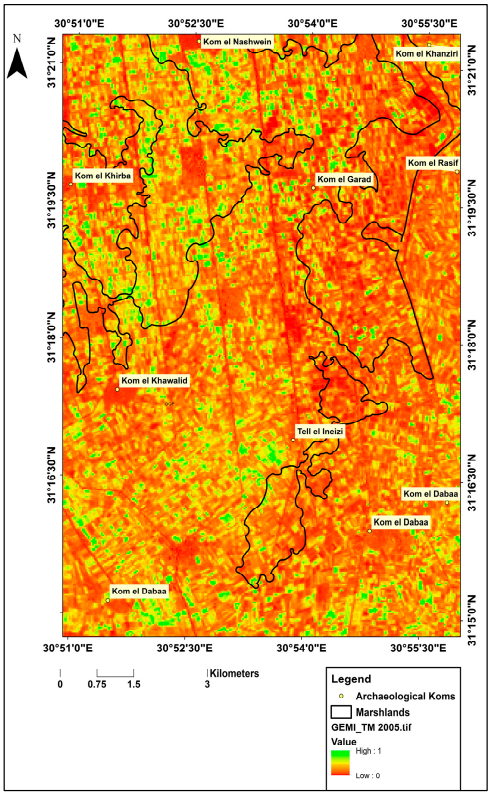
30°51'0"E
30°52'30"E
30°54'0"E
30°55'30"E
N
31°21'0"N
31°19'30"N
31°18'0"N
31°16'30"N
31°15'0"N
Kom el Nashwein
Kom el Khanziri
Kom el Khirba
Kom el Garad
Kom el Rasif
Kom el Khawalid
Tell el Inezi
Kom el Dabaa
Kom el Dabaa
Kom el Dabaa
0 0.75 1.5 3 Kilometers
Legend
Archaeological Koms
Marshlands
GEMI_TM 2005.tif
Value
High : 1
Low : 0

(**d**)

Figure 4. Images illustrating ancient marshland area appearing in orange-red color (low value) referenced to the 1941 topographic map using remote sensing indices: (**a**) EVI2 index with Landsat satellite image MSS 1973; (**b**) GNDVI index with Landsat satellite image MSS 1978; (**c**) OSAVI index with Landsat satellite image MSS 1988; (**d**) GEMI index with Landsat satellite image TM 2005.

3.3. The Results of the Sentinel-1 (C-Band)

In this study, we tested the suitability of the observations of the Sentinel-1 interferometric wide swath (IW) acquisition mode for detecting the potential areas for settlements in wetland using SAR data. In order to achieve our aim, the data were analyzed using apply orbit file, radiometric calibration, multilooking, speckle filtering, and geometric terrain correction. Two Sentinel-1 images (GRD) were tested, i.e., S-1A May 2018 and S-1B May 2019. The results of the investigated imagery dates showed that the composite value could be seen using the Intensity VV+VH and Amplitude VV+VH. A calibration vector allowed a simple conversion to be made of image intensity values into sigma0 values (Sigma0_VV and Sigma0_VH), the most suitable polarization for showing the potential settlements in this study is the Sigma0_VV value. The final analyzed sentinel-1A, B, 2018, and 2019 images revealed three separate areas of a possible ancient settlement that were previously unknown (Figure 5a,b).

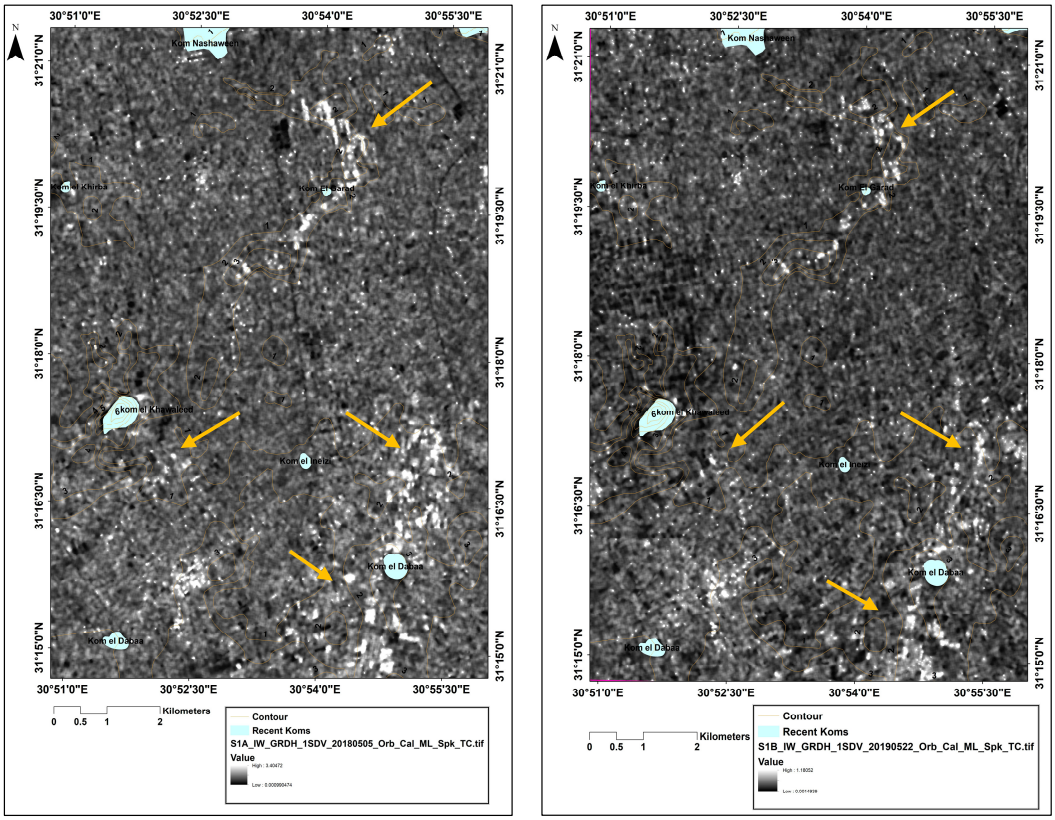

Figure 5. Potential areas of ancient architecture in association with known archaeological koms as discerned in the C-band Sentinel-1 Synthetic Aperture Radar (SAR) data: (**a**) Sentinel-1 image captured on 5 May 2018; (**b**) Sentinel-1B image captured on 22 May 2019.

4. Discussions

In this study, the topographic maps (1722, 1941, 1950, and 1997), Optical Corona (1965), Landsat MSS (1973, 1978, and 1988), TM (2005) data, and Radar SRTM (2014) and Sentinel1 (2018 and 2019) data have been used to demonstrate the capabilities of using an integrated data method to identify

potential buried settlement sites in the Nile Delta. In general, the topographic maps can give information about some features that have since disappeared according to the changes in the land use/land cover [65]. Also, the reflected vegetation value from the band indices techniques in the optical satellite images can give accurate information about land cover classes [66]. On the other hand, the radar (Sentinel1) data is unimpeded by clouds and can help in detecting buried features based on minor variations in soil properties including moisture retention, crop history, and soil matrix that may be indicative of subsurface or destroyed archaeological features [67].

According to the results of this study, the analysis of the topographic maps between 1941 and 1997 showed that the marshlands area increased by about 5.5 km² between 1941 and 1950, and increased again by about 57.8 km² between 1950 and 1997. In conjunction with this increase of marshlands, the barren lands decreased by about 5.5 km² between 1941 and 1950, and decreased again by about 57.8 km² between 1950 and 1997. After the 1952-revolution, there was a policy of increased agricultural production through horizontal expansion into the desert and barren lands [68]. According to the changes in the barren land area in the analyzed topographic maps between 1941 and 1997, the barren lands were higher than the surrounding marshlands and all of these barren lands except for an area of 9.3 km² became cultivated lands. This enormous change in the land use in the study area led to these barren lands being covered with the vegetation. Four optical satellite images were also used to detect the original marshlands. The enormous changes in the land use/land cover in the study area could be observed using Corona data from 1965 (most of the total space of the discovered areas were still barren land with some signs that show the ancient boundaries of the original koms) and the subsequent dates of Google Earth images between 1984 and 2016 (Figure 6a-d).

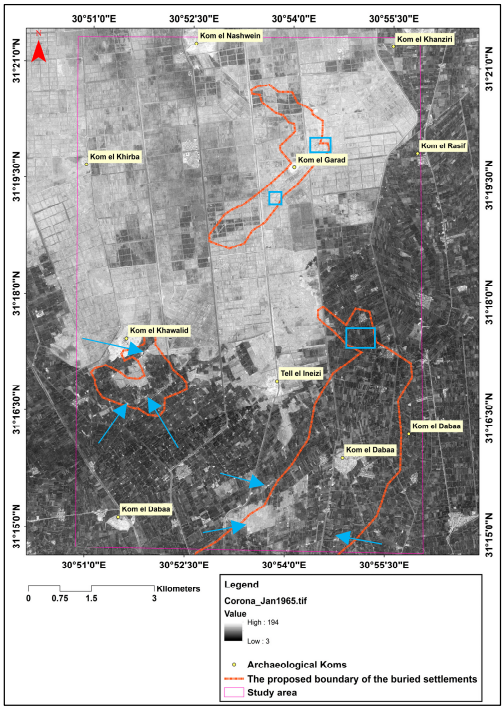

(**a**)

(**b**)

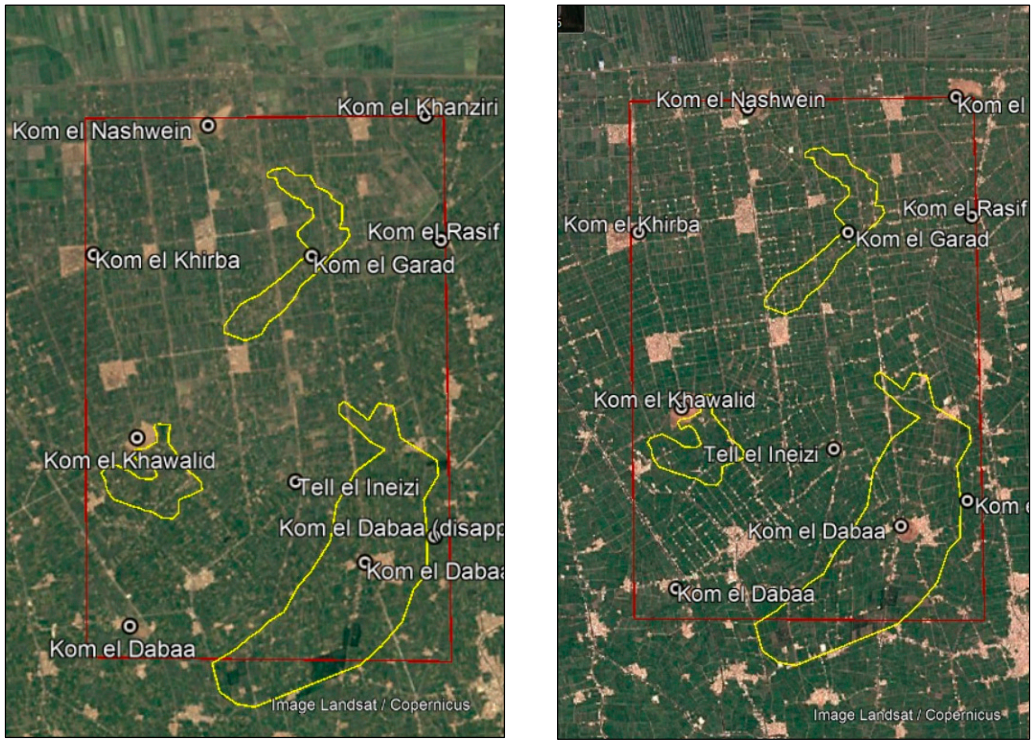

(**c**) (**d**)

Figure 6. Images illustrating changes in land use/land cover in the study area between 1965, 1984, 1995, and 2016: (**a**) Corona satellite image from 1965 (with arrows and squares indicating signatures associated with the original koms); (**b**) Landsat/Copernicus, Google Earth image from 12/1984; (**c**) Landsat/Copernicus, Google Earth image from 12/1995; (**d**) Landsat/Copernicus, Google Earth image from 12/2016.

In the 19th century, Sir William Smith referenced the Diocese of Buto (Butos in Greek language) that corresponds to the Ancient city of Buto in the Nile Delta, and noted that north of the town of Buto was a lagoon formed by the Nile near its junction with the Mediterranean Sea has that was likewise named Buto Lake; within the lake was the islet of Chemmis [69]. Further, some bishops of Buto from between 431 and 459 AD [70] are named in Worp's list of Byzantine bishops in Egypt [71]. The oldest named lake that corresponds to Lake Buto is Lake Borullus [72]. Herodotus described the island of Chemmis as lying in a deep and wide lake near to the temple at Buto [73]. In Figure 7, the 1772 Diocese of Buto map illustrates the situation of Buto (and the study area) set within the delta channels of the Nile. This map illustrates the dramatic changes in the hydrographic landscape of the study area, and helps explain why much of the ancient landscape and human occupation could be buried in alluvium or otherwise destroyed by the rechanneling of distributaries, and is now invisible to normal surface and aerial photographic survey (Figure 7a,b).

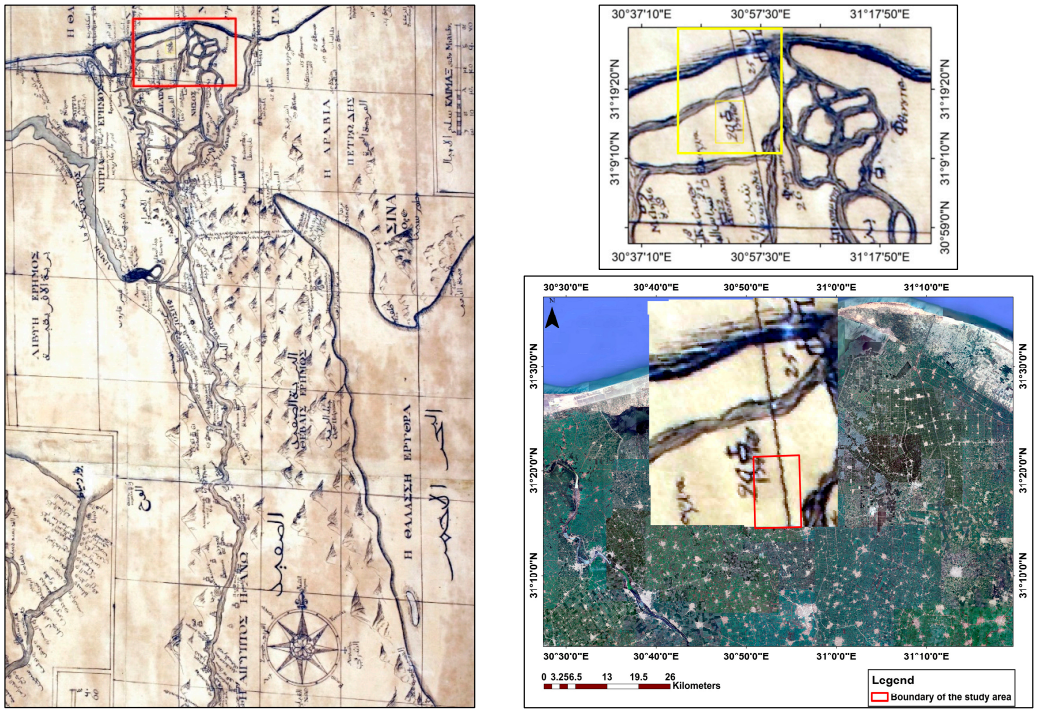

(**a**) (**b**)

Figure 7. Shows the location of the study area and the ancient Diocese of Buto: (**a**) the map of Egypt with the ancient towns and Dioceses in 1722 [74]; (**b**) the boundary of the study area matched with the georeferenced strip of the topographic map and Google image.

As an initial step, the seasonally (January, May, July, and October) -available satellite imagery was processed to test the optimal time for data collection. It was determined that May provided the best data for analysis in the studied years. The key variables related to the quality of the imagery were the agriculture seasons (harvest season and dry soil) [75,76], the climate conditions (a clear sky without fogs or clouds), the satellite image sensor properties (perfect condition for the image capture), and, of course, the availability of data collected over the study area which, for May, included Landsat optical and Sentinel1 radar imagery. In the same context, four-band combination methods were applied to the Landsat satellite images. EVI2 index was applied to the Landsat MSS 1973, GNDVI index to the Landsat MSS 1978, OSAVI index to the Landsat MSS 1988, and GEMI index to the Landsat TM 2005. Because this study is focused on detecting ancient occupations, these remote sensing indices served as a proxy to measure the differences in the vegetation value between the original marshland and barren area in the study area. By using combinations of the relevant indices (EVI2, GNDVI, OSAVI, and GEMI), we were able to take advantage of recent methodological enhancements in land use mapping [77]. The results of the remote sensing indices showed that the marshlands identified correlated significantly with the historic topographic maps. The marshlands and the current koms appeared orange-red in color, while the original barren lands (according to the maps), appeared green. The range-red color in the processed satellite images links with the heavy accumulations of salts in the koms and marshlands [78]. Generally, it was observed that in EVI2 (1973), the total reflected signature had a wider boundary than the identified settlements areas. This appears to capture the agricultural reclamation at an early stage (Figure 6a). On the other hand, the congruence between the proposed boundary and the area with low vegetation value in NDVI 1978 image is clearer than the EVI2 (1973), with the most significant indicator from the investigated images occurs on the OSAVI (1988) data. This image captured the regional impact after 36 years of the reclamation process in the Nile Delta. However, a human enhancement to the soil blurred the actual boundaries impacting the congruence between the proposed feature area and the suggested settlement areas in the GEMI (2005) imagery. All of the investigated images using indices techniques

yielded low values in the areas of recent tells; the variance between these images can be explained by the anthropogenic processes of reclamation and soil enhancement in recent decades. The disparity in the land topography in the current study (having about 10 potential archaeological sites around the potential settlements areas) suggests the presence of significant occupation features under the recent urban and agriculture lands.

The SRTM data was used to detect the differences in surface elevation in the study area which demonstrated that the potential settlement areas (5–7m) have a higher value than the surrounded areas about 2 or 3m. It was observed that the study area was situated at three main elevations between one and thirteen meters. The first level, between 1–2m, represents the total elevation of the agriculture land. The second level, between 5–7m, clearly demarks the total selected areas as possible archaeological sites. The third level, between 9–13m, represents known archaeological tells. In general, the elevation data collected in the interstitial areas do not provide evidence of archaeological features, whereas known tell sites with the highest elevation and the suggested sites with an elevation between 5–7m do indicate known and a possible history of ancient architecture. These results support the notion that the selected areas are candidates for buried archaeological features now hidden in the floodplain alluvium which has accumulated an overburden of Nile silt (up to 6m) and a general rise in the water table, which would place the deeper archaeological features below well below the water table [79] (Figure 8).

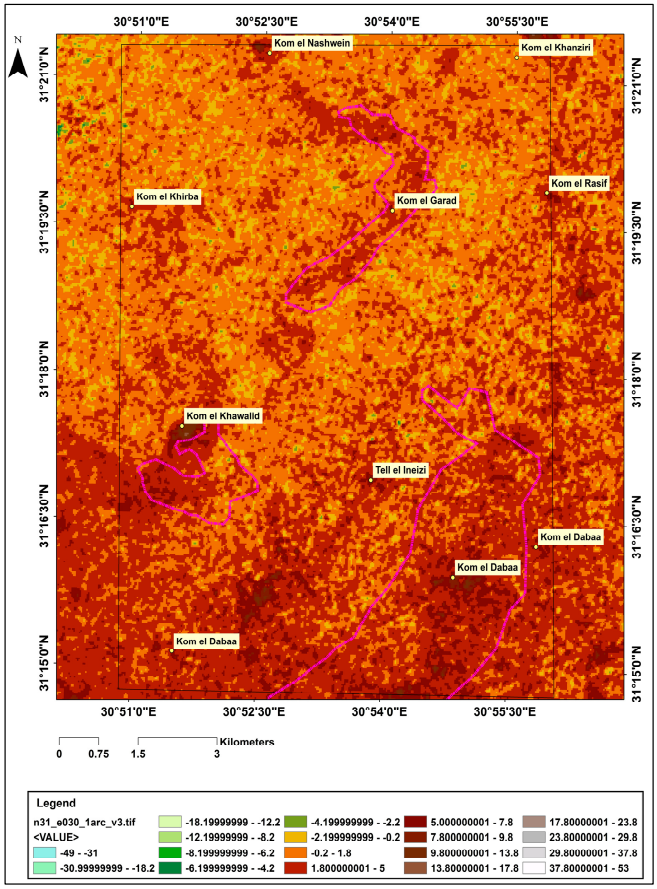

Figure 8. Shows the SRTM DEM data illustrating the difference in the elevation between the three discovered sites and the surrounding lands.

Sentinel-1 (c-band) data were analyzed to detect buried material in the study area. As the result of the large size of the potential discovered areas and the previous results of the ancient topographic maps integrated with the optical imagery, the results of the analyzed Sentinel1-A May 2018 and

Sentinel1-B May 2019 data suggest that the barren lands observed in 1941 and 1950 could have been occupations in ancient times. This supposition is supported by the identification of three separate areas of possible occupation. These discovered features are not completely contiguous in every area, and they appear in discrete blocks. The first discovered area covers about 12.2 km², the second covers about 3.12 km², and the third covers about 2.2 km². Furthermore, after the matching between the extracted layers of the maps, the optical data, and the Sentinel1 radar data, the results of the study support a theory that the old barren lands were relicts of ancient landscapes associated with human occupation [80]. According to the changes in the land-use/land-cover in the last eighty years, most of these ancient lands have since been transformed into cultivated lands (Figure 9a-d). One of the main results of our study is that it highlights that the koms are just part of ancient settlement patterns and land use, rather than the complete sites.

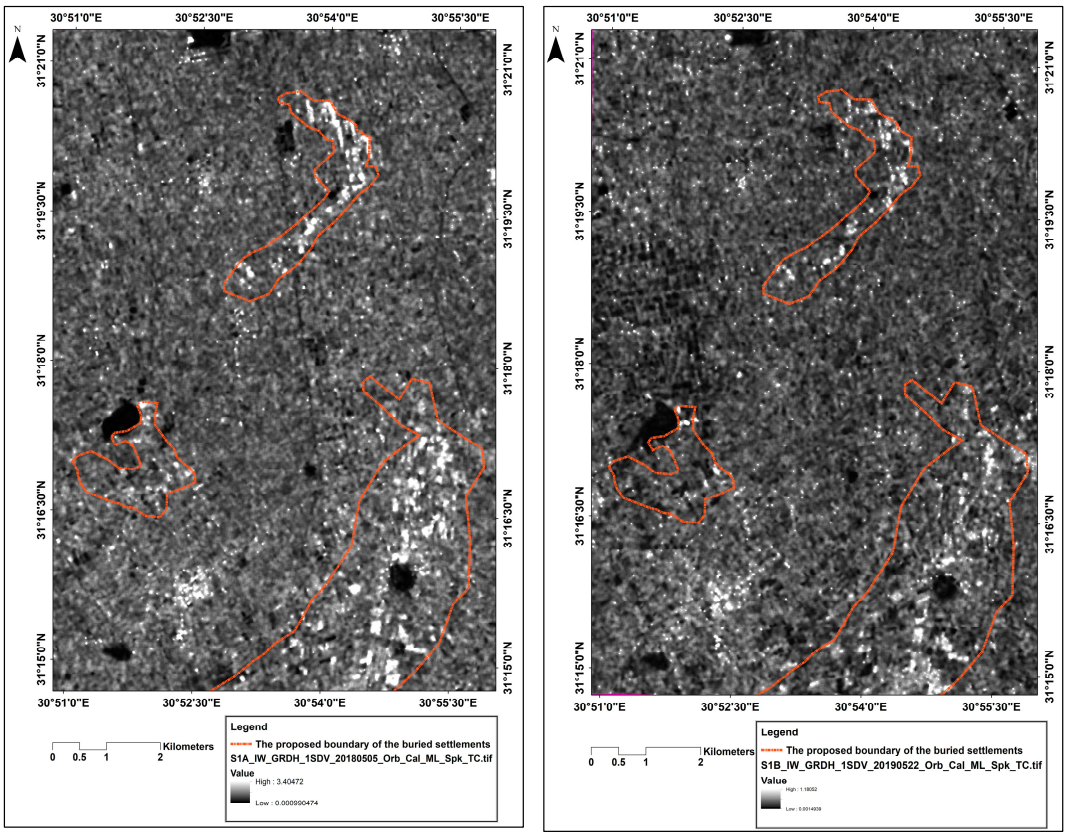

(**a**) (**b**)

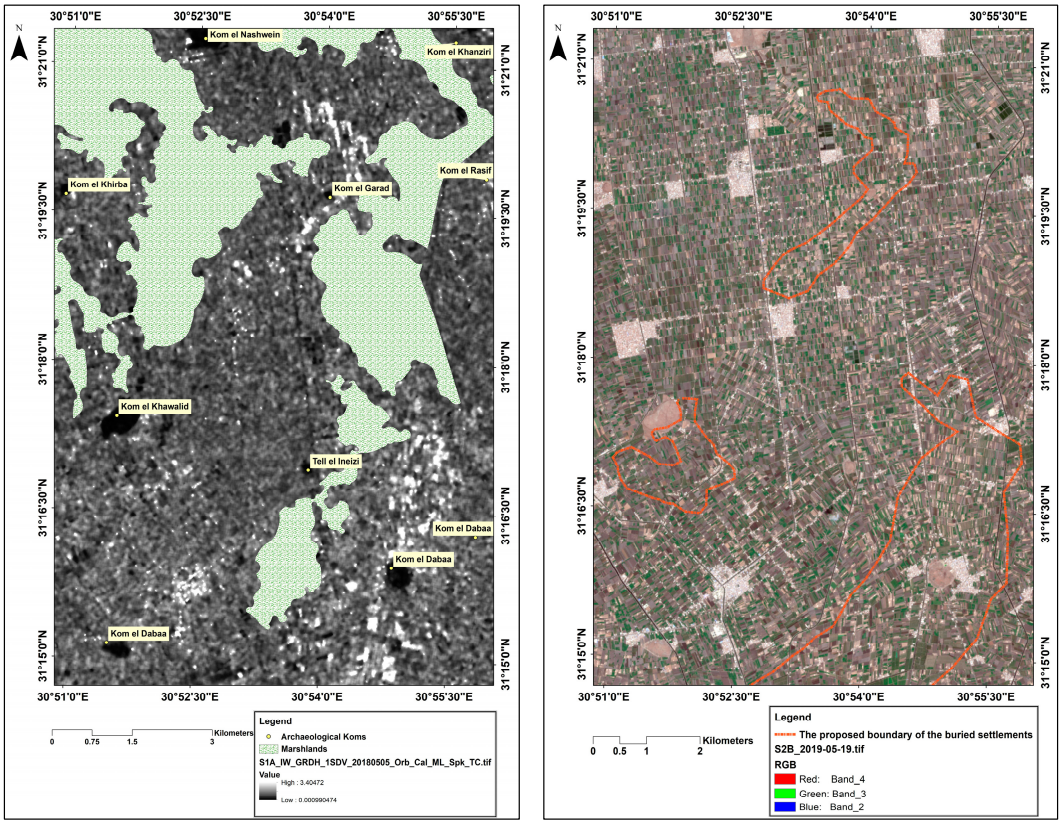

(**c**) (**d**)

Figure 9. Shows overall view of the study area: (**a,b**) potential areas of ancient constructions derived from i2018 and 2019 images using C-band Sentinel1 data; (**c**) the extent of the marshland according to the 1941 topographic map; (**d**) possible areas of settlement/ancient land-use overlaid on current Landsat/Copernicus satellite image, Google Earth 2019.

During the field survey, one farmer told the team that he found traces of what may have been archaeological remains (outside the area to the north-east). The farmer was digging a canal for irrigation. At a depth of about four meters within the cultivated land, he encountered some stone/ burnt brick remains. The stones/ burnt bricks seemed to form a chamber about 3 x 2.5m, with a height of about 3m. The team recorded the geographic coordinates of the room and, after that, we matched the coordinates with the radar image. According to the radar data, the geographical site of the room gave a similar spectral signature of the three detected areas. So, it is proposed that areas discovered through the image analysis with a matching signature of that of the area where the buried structure may likewise have buried building materials (Figure 5a,b). This is consistent with the results of Wilson and Ginau et al., which suggested that the archaeological remains of the ancient sites mainly flanked the river channel branches favoring the higher elevated levees along the paleochannels; locales favorable for settlement [81,82].

Until the 1960s, the summer inundation deposited an annual layer of alluvium over the flat alluvial plain of the Delta. These deposits caused the disappearance of the earlier channels of the river and accumulated around areas of ancient occupations including prehistoric sites and structures of historic times [68]. During the last seven thousand years, humans modified the delta landscape considerably. Some of the most conspicuous results of his activities are the koms, which are mostly the accumulated debris of thousands of years of human occupation, and are only occasionally related to natural effects [68]. In the pharaonic period, Lower Egypt was a territory where a powerful early kingdom was established, with settlements located on low, sandy knolls called turtlebacks that rose above the floodplain, especially noted in the eastern Delta [83]. The area of Hyksos settlement in the

eastern Delta, rulers who extended their control over Egypt during the Fifteenth Dynasty, also lay beneath some of the most fertile agricultural ground in Egypt. The expansion of modern agricultural lands and settlements likewise obscured these important northern Egyptian sites [84]. From the beginning of the Nineteenth Dynasty, the eastern frontier of the Delta, the weakest point of Egyptian defenses, was protected by a series of fortified settlements similar to those of Canaan [85]. In the same context, Herodotus (historian c. 484 BC- 425 BC) said, "the elevations (islands in Delta Nile), which are the work of man, are crowned for the most part with the white walls of towns and villages" [86]. According to the outputs of the topographic maps, optical imagery, radar data, the discovered chamber, and the scientific references, solid materials (e.g. limestone or burnt brick) have been used in construction in the three discovered areas. The lack of chronological control means that these three detected sites could date to any period, from the Middle kingdom, Hyksos, or most likely, to the Ptolemaic or Roman periods (Figure 10a,b).

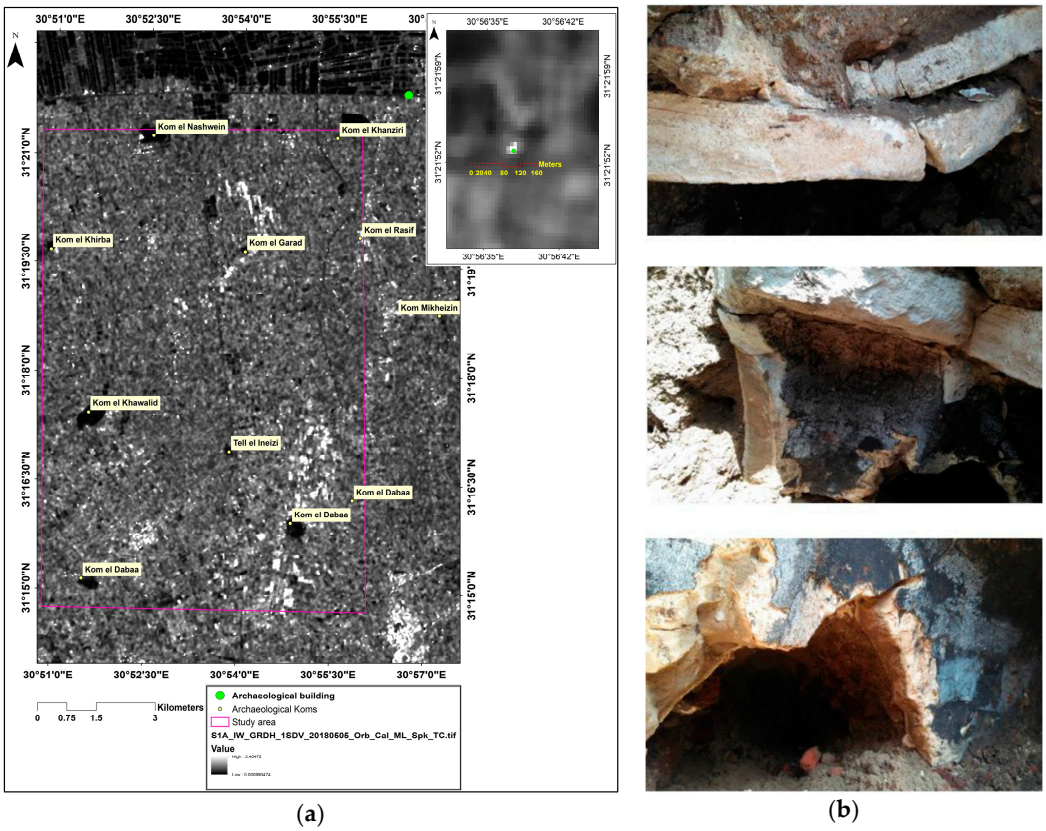

Figure 10. Shows an undated archaeological structure exposed by farmers in 2018: (**a**) the area of the structure and corresponding signature on C-band Sentinel1 data; (**b**) photograph from ground-truth field survey including views the ceiling and inside the chamber.

5. Conclusion

The current improvements in earth observation technologies offer advanced technical characteristics that enable new applications of methods specifically designed for the documentation, discovery, and risk monitoring of cultural heritage. In particular, the most recent space missions such as the European Space Agency (ESA) Sentinel-1 A, B are specifically concerned with flooding studies and heritage prospection, and have been systematically acquiring data for the entire globe [87]. This study explores the possibility of integrating historical topographic maps, optical, and radar data for the detection of ancient landscapes and sites in Egypt. The results of the topographic map analysis helped in detecting the changes in the land-use/land-cover between 1941 and 1997. Also, the changes in the land use/land cover between 1965 and 2016 were detected by integrating the optical Corona

data from January 1965, and the Google Earth Images (1984, 1995, and 2016). Evidence of changes in the original boundaries of the ancient koms and tells were detected using Corona data from 1965. In the same context, four types of remote sensing indices were applied in Landsat MSS 1973, 1978, 1988, and TM 2005 to detect the original marshlands. Radar SRTM data was used to identify the disparity in the elevation and topography between the potential settlement areas and the surrounding lands. By correlating older topographic maps with the Sentinel-1 radar outputs, we were able to analyze variations between the higher elevation and low-lying lands and compare contours derived from multiple sources. Overall, the results indicate that the areas identified from the radar Sentinel1 as potential settlements are very close to the lost areas around Lake Buto (Diocese of Buto) correlate with the barren land in the 1941 topographic map, the areas with low vegetation values in the investigated optical images using band indices techniques, and the higher elevation lands in the SRTM data. Furthermore, the higher elevation areas in the SRTM data tend to be larger than the selected areas in the radar data, because the Sentinel1 data indicated a reflectance from possible architectural remains yielding the solid in white color. Areas identified based on elevation could represent areas of ancient activity that lack architectural remains due to the land-use history, and thus, that would not be detected by the Sentinel1 data. Likewise, the same reasoning can be applied to the topographic and optical data. In the same context, some observed areas in Sentinel1 data are not completely contiguous, so some green strips (no indication of settlement) are observed inside the suggested areas as settlements based on the optical data. In this study, we applied a multifaceted study of various sources of high-quality landscape mapping to build a general vision of the modern and ancient geomorphological and topographic dynamics of landscapes of the Delta civilizations. Unlike much of the theoretical thinking about the ancient civilization of the Nile Delta, this study is a further step in expanding the concept of koms into a larger variegated settlement landscape which takes into account the paleogeography of the region. The integration between all available and accurate data (e.g., the old topographic maps, optical, and radar data) can help in the heritage studies by monitoring landscape changes. A multidisciplinary team that includes archaeologists and remote sensing specialists can enhance the ability to design research projects that can explore the potential of remote sensing data in the study of ancient settlement patterns and, consequently, the development of socio-political complexity. While not conclusive and lacking chronological control, the results of this study provide a useful guide for the planning of excavation missions that can increase the efficiency of limited resources for archaeological exploration. From data like this, the Ministry of Antiquities can decide how best to direct their resources and rescue efforts associated with further development projects that threaten otherwise buried archaeological heritage sites.

Improving and enhancing the methods used in analyzing the ever-more available optical and radar data is one of our primary goals, and in the next phase of this project, we will focus on detecting the ancient landscape in the whole of Kafr El Sheikh Governorate.

Author Contributions: The research article included three main contributions; archaeological view, data analysis, and writing the manuscript. A. E, M. A. R. A, R. E, P. W, Ch. M, and J. S provided the archaeological view. The maps and remote sensing imagery have been analyzed by R. L, A. E, and W. M. The manuscript has been written by A. E, M. A. R. A and R. L. The last version of the article has been revised by R. L, P. W., Ch. M, M. A. R. A, A. E, and J. S.

Funding: Authors would like to declare that the funding of the study has been supported by the authors' institutions.

Acknowledgments: The authors would like to thank the Italian National Research Council (CNR) at Tito Scalo, Potenza for supporting the research activities. Special thanksgiving to National Authority for Remote sensing and Space science (NARSS) for supporting the research activities. Also, many thanks are giving for the University of Kafrelsheikh (KFS), Egypt for supporting the excavation team in Buto (Tell el-Farain), which helped in achieving these results.

Conflicts of Interest: The authors would like to hereby certify that no conflict of interest in the data collection, processing the data, the writing of the manuscript, and in the decision to publish the results.

References

1. Bard, K.A. The Egyptian Predynastic: A review of the evidence. *J. Field Archaeol.* **1994**, *21*, 265–288, doi:10.1179/009346994791547553.
2. Lippiello, L.E. *Landscapes of Ancient Egyptian Religion: Rock Art as Indicator for Formal Ritual Spaces during the Formative Stage of the Egyptian State*; Yale University: New Haven, Connecticut, 2012.
3. Bard, K.A. The geography of excavated Pre-dynastic sites and the rise of complex society. *J. Am. Res. Cent. Egypt* **1987**, *24*, 81–93, doi:10.2307/40000263.
4. Kaelin, O. Gods in Ancient Egypt. In *The Oxford Research Encyclopedia of Religion*, (oxfordre.com/religion); Oxford University Press: Oxford, UK, 2016, doi:10.1093/acrefore/9780199340378.013.244. Available online: https://oxfordre.com/religion/abstract/10.1093/acrefore/9780199340378.001.0001/acrefore-9780199340378-e-244 (accessed on 14 December 2019).
5. Stanley, D.J.; Warne, A.G. Nile Delta: Recent geological evolution and human impact. *Science* **1993**, *260*, 628–634.
6. Stanley, D.J.; Warne, A.G. Sea level and initiation of Predynastic culture in the Nile delta. *Nature* **1993**, *363*, 435.
7. Arbouille, D.; Stanley, D.J. Late Quaternary evolution of the Burullus lagoon region, north-central Nile delta, Egypt. *Mar. Geol.* **1991**, *99*, 45–66.
8. Zimerle, B.K. *Before the Pyramids: The origins of Egyptian Civilization*; Teeter, E., Ed.; Oriental Institute of the University of Chicago: Chicago, IL, USA, 2011; pp. 1–288.
9. El Beialy, S.Y.; Edwards, K.J.; El-Mahmoudi, A.S. Geophysical and palynological investigations of the Tell El Dabaa archaeological site, Nile Delta, Egypt. *Antiquity* **2001**, *75*, 735–744.
10. Lange-Athinodorou, E. Palaces of the Ancient Mind: The Textual Record versus Archaeological Evidence. 2018. pp. 39–63. Available online: https://www.academia.edu/36185472/Palaces_of_the_Ancient_Mind_the_textual_record_versus_archaeological_evidence (accessed on 14 December 2019).
11. Mączyńska, A. *The Nile Delta as a Centre of Cultural Interactions Between Upper Egypt and the Southern Levant in the 4th Millennium BC*; Poznań Archaeological Museum: Poznań, Poland, 2014; pp. 1–320.
12. Steindorff, G.; Steele, K.C. *When Egypt Ruled the East*; University of Chicago Press: Chicago, IL, USA, 2014; pp. 1–304.
13. Geller, J. From prehistory to history: Beer in Egypt. In *The Followers of Horus (Egyptian Studies Association Publication 2)*; Oxbow: Oxford, UK, 1992; pp. 19–26.
14. Chyla, J., 2017. How Can Remote Sensing Help in Detecting the Threats to Archaeological Sites in Upper Egypt?. Geosciences, 7(4), p.97.
15. Sparavigna, A.C. The Satellite Archaeological Survey of Egypt. 2011. *arXiv* **2011**, arXiv:1105.6315. Available online: https://docs.google.com/document/d/19nFCK6zqeNFnGPub1y7ttwi57lYDQ6VrDuATrfi5T3k/edit (accessed on 14 December 2019).
16. Lasaponara, R.; Masini, N. Satellite synthetic aperture radar in archaeology and cultural landscape: An overview. *Archaeol. Prospect.* **2013**, *20*, 71–78, doi:10.1002/arp.1452.
17. Elfadaly, A.; Lasaponara, R. On the Use of Satellite Imagery and GIS Tools to Detect and Characterize the Urbanization around Heritage Sites: The Case Studies of the Catacombs of Mustafa Kamel in Alexandria, Egypt and the Aragonese Castle in Baia, Italy. *Sustainability* **2019**, *11*, 2110, doi:10.3390/su11072110.
18. Elfadaly, A.; Attia, W.; Lasaponara, R. Monitoring the Environmental Risks Around Medinet Habu and Ramesseum Temple at West Luxor, Egypt, Using Remote Sensing and GIS Techniques. *J. Archaeol. Method Theory* **2018**, *25*, 587–610, doi:10.1007/s10816–017–9347-x.
19. Elfadaly, A.; Attia, W.; Qelichi, M.M.; Murgante, B.; Lasaponara, R. Management of Cultural Heritage Sites Using Remote Sensing Indices and Spatial Analysis Techniques. *Surv. Geophys.* **2018**, *39*, 1347–1377, doi:10.1007/s10712-018-9489-8.
20. Elfadaly, A.; Lasaponara, R.; Murgante, B.; Qelichi, M.M. Cultural Heritage Management Using Analysis of Satellite Images and Advanced GIS Techniques at East Luxor, Egypt and Kangavar, Iran (A Comparison Case Study). In Proceedings of the International Conference on Computational Science and Its Applications, Springer, Cham, Trieste, Italy, 19 July 2017; pp. 152–168. doi:10.1007/978-3-319-62401-3_12.
21. Elfadaly, A.; Wafa, O.; Abouarab, M.A.; Guida, A.; Spanu, P.G.; Lasaponara, R. Geo-Environmental Estimation of Land Use Changes and Its Effects on Egyptian Temples at Luxor City. *ISPRS Int. J. Geo-Inf.* **2017**, *6*, 378, doi:10.3390/ijgi6110378.

22. Lasaponara, R.; Murgante, B.; Elfadaly, A.; Qelichi, M.M.; Shahraki, S.Z.; Wafa, O.; Attia, W. Spatial open data for monitoring risks and preserving archaeological areas and landscape: Case studies at Kom el Shoqafa, Egypt and Shush, Iran. *Sustainability* **2017**, *9*, 572, doi:10.3390/su9040572.
23. Lasaponara, R.; Elfadaly, A.; Attia, W. Low cost space technologies for operational change detection monitoring around the archaeological area of Esna-Egypt. In Proceedings of the International Conference on Computational Science and Its Applications, Springer, Cham, Beijing, China, 4–7 July 2016; pp. 611–621, doi:10.1007/978-3-319-42108-7_48.
24. Chen, F.; Masini, N.; Yang, R.; Milillo, P.; Feng, D.; Lasaponara, R. A space view of radar archaeological marks: First applications of COSMO-SkyMed X-band data. *Remote Sens.* **2015**, *7*, 24–50, doi:10.3390/rs70100024.
25. Tapete, D.; Cigna, F. Urban remote sensing in areas of conflict: TerraSAR-X and Sentinel-1 change detection in the Middle East. In *Fourth International Conference on Remote Sensing and Geoinformation of the Environment (RSCy2016)*; International Society for Optics and Photonics (Paphos, Cyprus): 2016; Volume 9688, p. 968821.
26. Chen, F.; Lasaponara, R; Masini, N. An overview of satellite synthetic aperture radar remote sensing in archaeology: From site detection to monitoring. Journal of Cultural Heritage, **2017**, 23, pp.5-11..
27. Tapete, D. Remote sensing and geosciences for archaeology. *Geosci. J.* **2018**, *8*, 41, doi:10.3390/geosciences8020041.
28. Lange, E.; Ullmann, T.; Baumhauer, R. Remote Sensing in the Nile Delta: Spatio-tempoRal Analysis of BuBastis/Tell Basta. Ägypten und Levante/Egypt and the Levant. *Ägypten und Levante* **2016**, *26*, 377–392, doi:10.1553/AEundL26s377.
29. Trampier, J. *Ancient Towns and New Methods: A GIS and Remote Sensing—Guided Archaeological Survey in the Western Nile Delta*; Chicago, USA, 2009, doi: 10.6082/M1WH2N5X.
30. Branting, S.; Trampier, J. Geospatial data and theory in archaeology: A view from CAMEL. *Space-Archaeol. Final Front.* **2007**, 272–289.
31. Trampier, J.R. *The Dynamic Landscape of the Western Nile Delta from the New Kingdom to the Late Roman Periods*; The University of Chicago: Chicago, IL, USA, 2010. Available online: https://www.academia.edu/352345/The_Dynamic_Landscape_of_the_Western_Nile_Delta_from_the_New_Kingdom_to_the_Late_Roman_Periods (accessed on 14 December 2019).
32. Parcak, S. Satellite remote sensing methods for monitoring archaeological tells in the Middle East. *J. Field Archaeol.* **2007**, *32*, 65–81.
33. Parcak, S.H. *Satellite Remote Sensing for Archaeology*; Routledge: London, UK, 2009, doi:10.1002/arp.373.
34. Parcak, S.; Mumford, G.; Childs, C. Using open access satellite data alongside ground based remote sensing: An assessment, with case studies from Egypt's Delta. *Geosciences* **2017**, *7*, 94.
35. Edwards, K.J.; Butzer, K.W. Early Hydraulic Civilization in Egypt: A Study in Cultural Ecology. *J. Hist. Geogr.* **1976**, *6*, 236.
36. Ozulu, İ.M.; Süel, M.; Tombuş, F.E.; Coşar, M. The Importance of Maps at the Archaeological Excavations Works. In Proceedings of the FIG Working Week, Rome, Italy, 6-10 May 2012.
37. Campana, S. Archaeological site detection and mapping: Some thoughts on differing scales of detail and archaeological 'non-visibility'. In *Seeing the Unseen. Geophysics and Landscape Archaeology*; CRC Press: Boca Raton, FL, USA, 2008; pp. 31–52.
38. Petrie, C.; Orengo, H.; Green, A.; Walker, J.; Garcia, A.; Conesa, F.; Knox, J.; Singh, R. Mapping Archaeology While Mapping an Empire: Using Historical Maps to Reconstruct Ancient Settlement Landscapes in Modern India and Pakistan. *Geosciences* **2019**, *9*, 11, doi:10.3390/geosciences9010011.
39. Scianna, A.; Villa, B. GIS applications in archaeology. *Archeol. Calcolatori* **2011**, *22*, 337–363.
40. Wahab, H.S.A.; Stanley, D.J. Clay mineralogy and the recent evolution of the north-central Nile delta, Egypt. *J. Coast. Res. Vol 7 No 2*, **1991**, 317–329.
41. Karyabwite, D.R. *Water Sharing in the Nile River Valley*; UNEP/DEWA/Grid: Geneva, Switzerland, 2000. Available online: http://nile.riverawarenesskit.org/english/nrak/Resources/Document_centre/UNEP_Water_Sharing_in_the_Nile_River_Valley_2000.pdf (accessed on 14 December 2019).
42. Gaber, H.M.; Bahnassy, M.H.; Suliman, A.S.; El-Bana, T.A. Agroecological assessment of land resources in Northern Nile Delta: A case study in Kafr El-Shikh governorate. *J. Agric. Sci. Mansoura Univ.* **2003**, *28*, 7485–7502.
43. USGS Home Page. Available online: https://earthexplorer.usgs.gov/ (accessed on 27 June 2019).

44. ESA Home Page. Available online: https://scihub.copernicus.eu/ (accessed on 27 June 2019).
45. Topographic Maps of Egypt. Available online: http://legacy.lib.utexas.edu/maps/ams/egypt/ (accessed on 14 September 2019).
46. Band Designations for the Landsat Satellites. Available online: https://www.usgs.gov/faqs/what-are-band-designations-landsat-satellites?qt-news_science_products=0#qt-news_science_products (accessed on 27 June 2019).
47. Pinty, B.; Verstraete, M.M. GEMI: A non-linear index to monitor global vegetation from satellites. *Vegetatio* **1992**, *101*, 15–20.
48. Mondal, P. Quantifying surface gradients with a 2-band Enhanced Vegetation Index (EVI2). *Ecol. Indic.* **2011**, *11*, 918–924, doi:10.1016/j.ecolind.2010.10.006.
49. Gitelson, A.A. Wide dynamic range vegetation index for remote quantification of biophysical characteristics of vegetation. *J. Plant Physiol.* **2004**, *161*, 165–173.
50. Steven, M.D. The sensitivity of the OSAVI vegetation index to observational parameters. *Remote Sens. Environ.* **1998**, *63*, 49–60.
51. All Data Products in the Sentinel1. Available online: https://sentinel.esa.int/web/sentinel/missions/sentinel-1/data-products (accessed on 27 June 2019).
52. User Guides for Sentinel-1-SAR Level-1. Available online: https://sentinel.esa.int/web/sentinel/user-guides/sentinel-1-sar/product-types-processing-levels/level-1 (accessed on 27 June 2019).
53. Fletcher, K. *SENTINEL 1: ESA's Radar Observatory Mission for GMES Operational Services*; European Space Agency: Paris, France, 2012.
54. Mancon, S.; Guarnieri, A.M.; Tebaldini, S. Sentinel-1 precise orbit calibration and validation. In Proceedings of the Fringe 2015: Advances in the Science and Applications of SAR Interferometry and Sentinel-1 InSAR Workshop, Frascati, Italy, 23–27 March 2015; pp. 1–4.
55. Twele, A.; Cao, W.; Plank, S.; Martinis, S. Sentinel-1-based flood mapping: A fully automated processing chain. *Int. J. Remote Sens.* **2016**, *37*, 2990–3004.
56. Level-1 Radiometric Calibration. Available online: https://sentinels.copernicus.eu/web/sentinel/radiometric-calibration-of-level-1-products (accessed on 27 June 2019).
57. Veloso, A.; Mermoz, S.; Bouvet, A.; Le Toan, T.; Planells, M.; Dejoux, J.F.; Ceschia, E. Understanding the temporal behavior of crops using Sentinel-1 and Sentinel-2-like data for agricultural applications. *Remote Sens. Environ.* **2017**, *199*, 415–426.
58. Liu, C. *Analysis of Sentinel-1 SAR Data for Mapping Standing Water in the Twente Region*; University of Twente, Enschede, Netherlands, 2016.
59. Weiß, T. SAR Pre-processing Documentation. 2018. Available online: https://buildmedia.readthedocs.org/media/pdf/multiply-sar-pre-processing/get_to_version_0.4/multiply-sar-pre-processing.pdf (accessed on 14 December 2019).
60. Abdurahman Bayanudin, A.; Heru Jatmiko, R. Orthorectification of Sentinel-1 SAR (Synthetic Aperture Radar) Data in Some Parts Of South-eastern Sulawesi Using Sentinel-1 Toolbox. In Proceedings of the IOP Conference Series: Earth and Environmental Science, Yogyakarta, Indonesia, 17–19 October 2016; Volume 47, p. 012007.
61. Adriansen, H.K. Land reclamation in Egypt: A study of life in the new lands. *Geoforum* **2009**, *40*, 664–674.
62. Small, D.; Schubert, A. Guide to ASAR geocoding. In *ESA-ESRIN Technical Note RSL-ASAR-GC-AD*; University of Zürich: Zürich, Switzerland, 2008; 1, p.36.
63. The Season of Wheat Harvesting in Egypt. Available online: https://ww.dailynewssegypt.com/2016/05/11/egypt-welcomes-season-wheat-harvesting/ (accessed on 16 Septembre 2019).
64. Dewidar, K.H.; Al Rehili, B. Assessment of vegetation indices for estimating plant coverage and plant density in the Northern Sarawat Mountains, Saudi Arabia. *Merit Res. J. Agric. Sci. Soil Sci.* **2013**, *1*, 19–32.
65. Statuto, D.; Cillis, G.; Picuno, P. Using historical maps within a GIS to analyze two centuries of rural landscape changes in Southern Italy. *Land* **2017**, *6*, 65.
66. Xu, N.; Tian, J.; Tian, Q.; Xu, K.; Tang, S. Analysis of Vegetation Red Edge with Different Illuminated/Shaded Canopy Proportions and to Construct Normalized Difference Canopy Shadow Index. *Remote Sens.* **2019**, *11*, 1192.

67. Tapete, D.; Cigna, F. Trends and perspectives of space-borne SAR remote sensing for archaeological landscape and cultural heritage applications. *J. Archaeol. Sci. Rep.* **2017**, *14*, 716–726.
68. Holz, R.K. Man-made landforms in the Nile Delta. *Geogr. Rev.* **1969**, *59*, 253–269, doi:10.2307/213457.
69. Smith, W. Dictionary of Greek and Roman Geography London. 1857. Available online: https://archive.org/details/dictionarygreek01smitgoog/page/n4 (accessed on 14 December 2019).
70. Le Quien, M. Oriens Christianus. In *Quatuor Patriarchatus Digestus: Quo Exhibentur Ecclesiae, Patriarchae, Caeterique Praesules Totius Orientis. Ecclesiam Maronitarum, Patriarchatum Hierosolymitanum, [et] Quotquot fuerunt Ritus Latini tam Patriarchae quam inferiores Praesules in quatuor Patriarchatus [et] in Oriente universo, complectens*; Tomus Tertius; ex typographia regia: Paris, France, 1740; Volume 3, pp. 539–540.
71. Worp, K.A. A checklist of bishops in Byzantine Egypt (AD 325-c. 750). *Zeitschrift für Papyrologie und Epigraphik* **1994**, 100, 283–318.
72. Dumont, H.J.; El-Shabrawy, G.M. Lake Borullus of the Nile Delta: A short history and an uncertain future. *AMBIO: A J. Hum. Environ.* **2007**, *36*, 677–683.
73. Mourad, S.A. From Hellenism to Christianity and Islam: The Origin of the Palm Tree Story concerning Mary and Jesus in the Gospel of Pseudo-Matthew and the Qur'an'. *Oriens Christ.* **2002**, *86*, 206–216.
74. Ecclesiastical Map of Egypt with Names in Greek and Arabic. Available online: http://www.bl.uk/manuscripts/FullDisplay.aspx?ref=Add_MS_5662 (accessed on 22 November 2019).
75. Hayes, W.C. *Most Ancient Egypt*; University of Chicago Press: Chicago, FL, USA, 1965; pp. 1–160. Available online: https://oi.uchicago.edu/sites/oi.uchicago.edu/files/uploads/shared/docs/most_ancient.pdf (accessed on 14 December 2019).
76. Ginau, A.; Schiestl, R.; Wunderlich, J. Integrative geoarchaeological research on settlement patterns in the dynamic landscape of the northwestern Nile delta. *Q. Int.* **2019**, *511*, 51–67.
77. Wilson, P. Human and Deltaic Environments in the Northern Egypt in Late Antiquity. *Late Antique Archaeol.* **2018**, *13*, 42–62.
78. Maisels, C.K. *Early Civilizations of the Old World: The Formative Histories of Egypt, the Levant, Mesopotamia, India and China*; Routledge: London, UK, 2003; pp. 1–504, doi:10.4324/9780203449509.
79. Hassan, F.A. The dynamics of a riverine civilization: A geoarchaeological perspective on the Nile Valley, Egypt. *World Archaeol.* **1997**, *29*, 51–74.
80. Bard, K.A.; Fattovich, R.; Ward, C. Sea port to punt: New evidence from Marsâ Gawâsîs, Red Sea (Egypt). *BAR INT. SER.* **2007**, *1661*, 143.
81. Bard, K.A. *An Introduction to the Archaeology of Ancient Egypt*, 2nd ed.; John Wiley & Sons: Hoboken, NJ, USA, 2015; pp. 1–480.
82. Alan, K.B.; Eugene Rogan. Egyptian agriculture in historical perspective. In *Agriculture in Egypt from Pharaonic to Modern Times*; (Proceedings of the British Academy 96, Oxford 1999); University of Oxford, Oxford, England, 1999; pp. xxviii + 427. ISBN 0–19–726183–3, doi:10.1017/S1047759400019541.
83. Mourad, A.L. Rise of the Hyksos: Egypt and the Levant from the Middle Kingdom to the early Second Intermediate Period. Ph.D. thesis, Sydney, Australia: Macquarie University 2014.
84. Bronn, J.A. Foreign rulers of the Nile: A reassessment of the cultural contribution of the Hyksos in Egypt. Ph.D. Thesis, University of Stellenbosch, Stellenbosch, 2006; pp. 1–127.
85. Maspero, G. *Manual of Egyptian Archaeology and Guide to the Study of Antiquities in Egypt: For the Use of Students and Travellers*; H. Grevel and Company: Putnam, NY, USA, 1895. Available online: https://archive.org/details/manualofegyptian00maspuoft/page/n6 (accessed on 14 December 2019).
86. Rawlinson, G. *History of ancient Egypt*; G. P. Putnam's Sons: New York, NY, USA; T. Fisher Unwin: London, UK; New York: John, B. Alden: 1886; Volume 2.
87. ESA Earth Observation Missions. Available online: https://earth.esa.int/web/guest/missions/esa-eo-missions (accessed on 16 September 2019).